Oxygen incorporation in Ti_2AlC thin films studied by electron energy loss spectroscopy and ab initio calculations

Aurelija Mockuté, Martin Dahlqvist, Lars Hultman, Per O A Persson and Johanna Rosén

The original publication is available at www.springerlink.com:

Aurelija Mockuté, Martin Dahlqvist, Lars Hultman, Per O A Persson and Johanna Rosén, Oxygen incorporation in T_2AlC thin films studied by electron energy loss spectroscopy and ab initio calculations, 2013, Journal of Materials Science, (48), 10, 3686-3691.
http://dx.doi.org/10.1007/s10853-013-7165-4

Oxygen incorporation in Ti_2AlC thin films studied by electron energy loss spectroscopy and *ab initio* calculations

A. Mockute,* M. Dahlqvist, L. Hultman, P.O.Å. Persson, and J. Rosen

Thin Film Physics Division, Department of Physics (IFM), Linköping University, SE-58183 Linköping, Sweden

*Corresponding author: Email-address: aurmo@ifm.liu.se, Tel.: +46 13 281279.

Substitution of C with O in hexagonal inherently nanolaminated Ti_2AlC has been studied experimentally and theoretically. $Ti_2Al(C_{1-x}O_x)$ thin films with $x \leq 0.52$ are synthesized by both cathodic arc deposition with the uptake of residual-gas O, and solid-state reaction between understoichiometric TiC_y and $Al_2O_3(0001)$ substrates. The compositional analysis is made by analytical transmission electron microscopy, including electron energy loss spectroscopy. Furthermore, predictive *ab initio* calculations are performed to evaluate the influence of substitutional O on the shear stress at different strains for slip on the (0001) basal plane in the [-1010] and [1-210] directions.

Keywords: MAX phases; Ab initio calculations; Electron energy-loss spectroscopy; Shear

1. Introduction

MAX phases belong to a family of ternary compounds with a general composition $M_{n+1}AX_n$, where *M* is an early transition metal, *A* is a group IIIA or IVA element, and *X* is C or N [1]. Following their initial discovery in the 1960s, MAX phases have gained increased attention as they exhibit both metallic and ceramic properties (good electrical and thermal conductors, shock resistant, hard, damage tolerant), which stem from the combination of metallic and covalent bonds and the characteristic nanolaminated structure [2,3].

The range of MAX phase properties can be further improved by alloying. Alloying on *M* and *A* sites has been extensively studied, and a large number of MAX phases synthesized,

with resultant change in, e.g., elastic properties and hardness of $Ti_3(Si,Al)C_2$ [4] and $(Ti.V)_2AlC$ [5], respectively, or conductivity in $(Ti,Nb)_2AlC$ [6]. Partial replacement of one element by another can also increase the stability, observed for $(Cr,V)_3AlC_2$ [7]. Solid solutions on the *X* site have also been investigated and, e.g., higher hardness of $Ti_2Al(C,N)$ as compared to both Ti_2AlC and Ti_2AlN has been observed [8]. Still, the alloying possibilities are limited due to only two elements available. However, a significant amount of O in Ti_2AlC has been reported [9,10], suggesting O as a potential *X* element besides C and N. These observations have motivated several theoretical studies, such as the influence of O on phase stability [11], O migration mechanisms in Ti_2AlC [12], O site/energy dependence on experimental conditions [12] and the effect of O on the electronic structure [12,13]. The calculations indicate that O prefers C site in Ti_2AlC under oxygen-lean conditions and high temperature [12] and that the concentration of the substitutional O could reach at least 15 at.% [11]. Furthermore, band structure analysis shows that the electronic structure of Ti_2AlC is anisotropic, being metallic in plane and insulating out of plane (in c-direction). A correlated change in Ti_2AlC conduction along the c-direction, from insulating via n-type to p-type, has also been suggested, for up to 12.5 at.% O [13]. Thus, a tunable anisotropic semiconductor could be obtained, promising for various technological applications, such as low friction electric contacts.

Ab initio calculations combined with electron energy loss spectroscopy (EELS) measurements have previously been used to confirm O incorporation on the C site in $Ti_2Al(C_{1-x}O_x)$ [14]. However, in order to experimentally confirm previous theoretical predictions and investigate the effect of composition on materials properties, a precise evaluation of the O content locally in high quality MAX phase is needed. So far, reported compositional analysis has been based primarily on elastic recoil detection analysis (ERDA). Care must be taken, as ERDA results contain contribution from grain boundaries and other structural imperfections, which may act as O getters, and can not be interpreted as reflecting the exact MAX phase composition. Furthermore, even though highly interesting electronic properties are predicted upon O incorporation, its effect on, e.g., mechanical properties needs to be further investigated.

Here, we report the range of O concentration attained in $Ti_2Al(C_{1-x}O_x)$ using two synthesis routes; deposition of Ti_2AlC_y by cathodic arc under high-vacuum conditions, and solid-state reaction following deposition of TiC_y films on $Al_2O_3(0001)$ substrates. The O content is determined by EELS, and shows an O range allowing tuning of the material's electronic and mechanical properties, as predicted by previous theoretical work and here presented first principles calculations.

2. Experimental

Thin films were synthesized using a high current pulsed cathodic arc source at a base pressure of $1 \cdot 10^{-6}$ mbar. Three center triggered cathodes were operated in alternating mode at a rate of 10 Hz, with pulse lengths set to 350, 300, and 850 μs for Ti, Al, and C, respectively. Prior to deposition $Al_2O_3(0001)$ substrates were rinsed in ethanol and degassed in the vacuum chamber at the growth temperature of 900ºC for 10 min. Pulse ratios of 15Ti : 10Al : 1C and 10Ti : 1C were used to deposit Ti_2AlC_y and understoichiometric TiC_y, hereafter referred to as Sample I and Sample II, respectively. Stoichiometric TiC is typically obtained using a 4:1 or 5:1 Ti:C pulse ratio, whereas 10:1 has been used for growth of Ti_2AlC [15,16]. Hence, *y* equals approximately 0.67 and 0.5 in Sample I and II, respectively. In Sample I, $Ti_2Al(C_{1-x}O_x)$ was obtained from Ti_2AlC_y deposited on stoichiometric TiC seed layer. Stoichiometric TiC does not favor decomposition of Al_2O_3 substrate, as opposed to understoichiometric TiC [14]. Thus, O in Sample I is primarily incorporated from residual gas, also confirmed by the comparatively sharp film-substrate interface. In Sample II, O was incorporated mainly as a result of Al_2O_3 decomposition with O interdiffusion between the substrate and the understoichiometric TiC_y film. A minor contribution of O from residual gas may be present also in Sample II, though suppressed by shorter deposition time between subsequent C layers.

X-ray diffraction (XRD) θ-2θ measurements were performed for phase identification using a Philips PW 1729 diffractometer equipped with a line focus Cu K_α source. The overall film composition was determined by ERDA. Significant incorporation of O was revealed throughout both samples, around 10 at.% and above. However, to exclude

effects from defects and grain boundaries and investigate the O content within the actual MAX phase structure, complementary compositional analysis was performed through analytical transmission electron microscopy (TEM).

Samples for cross sectional microscopy were prepared by traditional cutting, gluing and mechanical polishing followed by Argon ion milling in a Gatan PIPS system. The Ar ions were accelerated by a 5 kV potential at a 5º angle with respect to the surface. Finally a gentle polishing step was performed to remove surface damage at 1.8 kV and 6º tilt. Electron microscopy was performed in a Tecnai G2 TF 20 UT FEG-TEM, which was operated at 200 kV for a 1.9 Å point resolution. A Gatan ENFINA parallel spectrometer was used for EELS, with a dispersion of 0.3 eV/ channel and a 1 mm entrance aperture. The convergence angle of the electron probe was 10.1 mrad and the acceptance angle 1.0 mrad. Spatially overlapping low and core loss spectrum images were recorded in (S)TEM mode (image coupled) from the samples and used to extract the fine structure of the core losses. Spectrum imaging was performed while shifting the ZLP during acquisition, continuously for low losses and at the spatial shift between subsequent spectra for core losses, according to the method for reducing noise proposed by Bosman [17]. Initially, the spectra were aligned using the first derivative of the Ti-L3 peaks and subsequently averaged into single spectra. After background removal the spectra were compensated for plural scattering. Quantification of the material constituents Ti and O was performed using standard cross sections embedded into the Gatan Digital Micrograph software.

3. Results and discussion

3.1. Quantification of oxygen

Ab initio calculations predict a change of 0.06 Å in c lattice parameter for x=0.75 in $Ti_2Al(C_{1-x}O_x)$ as compared to pure Ti_2AlC [11]. Hence, based on Braggs law, no major shift (2θ=0.05º) in XRD peak positions is expected for the acquired O concentrations, and therefore, no compositional analysis is attempted based on acquired XRD data. Peaks corresponding to TiC and Ti_2AlC were found in θ-2θ diffractograms of both samples. The TiC peak in Sample I originates from the seed layer and minor amount of intergrown

material (see Fig.1). Presence of Ti_2AlC in Sample II indicates a reaction between the TiC_y film and the Al_2O_3 substrate [14].

Fig. 1a and b shows cross-sectional TEM images of Samples I and II, respectively. Both films are entirely crystalline and exhibit the characteristic laminated dark/bright layered structure of epitaxially grown MAX phase [see Fig. 1c and d] with local inclusions of cubic TiC phase and stacking faults. The thickness of the films is 100 nm and 65 nm, respectively. For each sample, a well defined MAX phase area was identified and an EEL spectrum image was recorded from it to produce the spectra in Fig. 2.

The Ti $L_{2,3}$ edges appear strongest with an edge onset at 452 eV loss. Furthermore, the Ti L_1 edge is visible at 563 eV and the O K edge is located at 531 eV energy loss. The latter is composed of two peaks, the sharper one presented at 535 eV, followed by a broader peak at 542 eV. While the presence of the O-K edge does not imply that O is present in the MAX phase structure, the fine structure of the edge is similar to previous investigations [14], where it was shown that O assumes the C site in Ti_2AlC. Furthermore, the O-K and C-K edges are qualitatively similar (not shown) suggesting a similar environment of the two elements in the compound. The intensity of the O-K edge is similar in both samples, suggesting O concentrations of a comparable order.

In this study the C and Al signals were not recorded. The Al edge is located at very high or very low energies, and for C, the intensity of the signal may partly originate from contamination. This leaves signals from Ti and O, which give their relative concentrations. Considering that stoichiometric Ti_2AlC MAX phase is composed of 50 at.% Ti, 25 at.% Al, and 25 at.% C, the O content has therefore been evaluated by assuming a stoichiometric Ti content fixed at 50 at.%. This assumption is based on the calculated extraordinarily high formation energy of Ti vacancies in the Ti_2AlC structure [18].

Estimating the Ti and O relative concentrations by EELS, particularly for O, faces challenges as it is sensitive to the choice of cross-sectional model, superimposed signal

(ontop of the Ti-$L_{2,3}$ edge) and choice of energy window widths. Here, the Ti-$L_{2,3}$ edge is assumed to exhibit a slow Gaussian like modulation, starting just before the O-K edge onset and peaking at the Ti-L_1 edge. The intensity of the O edge was achieved by assuming a linearly changing background and that the signal would reach zero at 20 eV energy loss after the edge onset. Assuming a slow Gaussian like modulation of the Ti-$L_{2,3}$ edge and modeling the background by a linear change, slightly overestimates the composition. On the other hand, assuming that the signal reaches zero 20 eV after the edge onset is unlikely, which then underestimates the O content slightly. However, the estimation of the O content in the material is similar for all employed models and by a final choice of a Hartree-Slater cross section model, since it gives the least residual signal, and employing a reference-based quantification (assuming that Ti must be ~50%) of the O content results in a total of ~10 and ~13 at.% O in Samples I and II, respectively. This is comparable with results obtained by ERDA and suggests that all O is primarily incorporated into the MAX phase. No accumulation of O at grain boundaries or other structural imperfections could be detected to the resolution of the experiments. The higher O concentration in Sample II is likely the result of primarily O uptake from the decomposing Al_2O_3 substrate during solid-state formation of the Ti_2AlC phase [14]. However, a minor contribution may have come from initial O incorporation during deposition of the TiC_y layer.

No pronounced solid-state reaction between TiC seed layer in Sample I and the Al_2O_3 substrate was observed. As shown by Persson et al. [14], stoichiometric TiC does not react with Al_2O_3, and thus there is no O interdiffusion.

3.2. Simulated mechanical properties

Substitutional O content in Ti_2AlC of up to 13 at.% allows experimental exploration of material properties over a concentration range theoretically predicted to involve drastic changes in anisotropic electronic structure. We have therefore performed additional density functional theory (DFT) calculations to investigate how the same O concentration range affects the mechanical behavior.

Implemented within VASP [19,20], we used the projector augmented wave (PAW) method [21] and the Perdew and Wang (91) generalized gradient approximation (GGA) [22] for the exchange and correlation functional. Furthermore, a plane wave cutoff of 500 eV and a Γ-centered grid of 7x7x5 *k*-points were used, in accordance with previous work [13].

The anisotropic crystal structure of MAX phases results in limited deformation due to lack of sufficient easy slip systems [23]. Basal plane dislocations with a Burgers vector of b=1/3(11-20) were detected in Ti_3SiC_2 by TEM [24,25]. Furthermore, deformation modes for two basal slip systems, [1-210](0001) and [-1010](0001), have been theoretically studied in Ti_2AlC and Ti_2AlN [26,27]. The latter slip system had the lowest ideal shear strength and was concluded to be predominant for the resulting mechanical properties for these compounds.

Substituting C with O in Ti_2AlC has been shown theoretically [11] as well as experimentally [9,16]. In this work we have studied the effect of O on shearing, through the stress-strain relationship for the [-1010](0001) and [1-210](0001) shear systems. This is of importance for increasing the understanding of how mechanical deformation and structural instability can be modified by means of O. 2x2x1 supercells have been used for $Ti_2Al(C_{1-x}O_x)$ where x = 0.00, 0.25, and 0.50. The O configurations within the supercells can be found in Ref. [13]. Previously, an increase in Ti-Al bond strength, caused by incorporation of O, was found to increase the shear elastic constant c_{44}, while bulk, shear, and Young's moduli undergo minor changes [11,13]. Here, a series of incremental shear strain was applied for each shear path and after each strain step the unit cell was internally relaxed while constraining the applied strain.

In Fig. 3a the calculated shear stress at different strains is shown for [-1010](0001) (solid lines) and [1-210](0001) (dotted lines) slip of $Ti_2Al(C_{1-x}O_x)$. For Ti_2AlC, the ideal strength of 9 and 11 GPa occurs at a strain around 0.125 and 0.15, respectively, for the two shear paths. Evident from the graph, our results for Ti_2AlC are consistent with Liao et al. and corresponding analysis based on CASTEP [27]. It shows that deformation

occurs more easily in the [-1010] direction under strain, which suggests that this mode governs the lattice stability under shear deformation.

The difference in ideal strength for different shear directions can be explained by how the Ti-Al bonds change in the Ti_6Al prism, see Fig. 3b, upon applied strain. Generally, Ti-C bonds undergo small changes during deformation, while Ti-Al bonds break during basal-plane slip. For the [-1010](0001) shear mode, see Fig. 3c, one Ti-Al bond (Ti in red triangle) stretches and finally breaks at the ideal strength of 0.125. A new Ti-Al bond (Ti in red triangle) is thus formed. For Ti_2AlC under strain in the [1-210] direction, see schematic I of Fig. 3d, two Ti-Al bonds (to one Ti in each layer) stretch and finally break after the ideal strength of 0.15. At the same time two new Ti-Al bonds (to one Ti in each layer) are created. The lower ideal strength for the [-1010](0001) mode can thus be related to fewer Ti-Al bonds affected during deformation.

When O is incorporated into Ti_2AlC the ideal strength increases almost linearly for the two strain modes. According to Liao et al. [27] such effect, also observed when comparing Ti_2AlC and Ti_2AlN, may be explained by electronic structure analysis and an increased number of valence electrons (in the present work originating from O), likely strengthening the Ti-Al bonds. For unstrained Ti_2AlC, the Ti-Al bonding states (Ti-d and Al-p) range from -2.3 to -0.2 eV. For $x = 0.25$, these states shift down, into the range -2.6 to -0.5 eV, and for $x = 0.50$ even further, to -2.8 to -0.7 eV. This is accompanied with a decrease in Ti-Al bond length, from 2.89, 2.86, to 2.83 Å for $x = 0.00$, 0.25, and 0.50, respectively. As a consequence, the ideal strength of both slip directions increases, resulting in a material more resistant towards mechanical deformation.

Structural evolution upon [-1010](0001) shearing, see Fig. 3c, is independent on O concentration. However, for the [1-210](0001) shear system, two different paths of structural changes can be identified, see Fig. 3d. Path I, involving breaking/formation of two Ti-Al bonds simultaneously, occurs for pure Ti_2AlC, as mentioned above. In path II, for $x = 0.25$ and 0.50, one bond is being broken/formed at a time in two successive steps, involving the same Ti layer in both cases. The difference between $x = 0.00$ and $x \neq 0.00$

can be explained by the different *X* elements creating differences in electronic density, resulting in different Ti-Al bond strength. Ti-Al bonds where the Ti atom has a higher degree of C as nearest neighbors break more easily as compared to higher presence of O. This effect was only found for the [1-210](0001) shear system, involving breaking/formation of two Ti-Al bonds as compared to only one for [-1010](0001).

4. Materials optimization

Previously reported calculations on phase stability of Ti_2AlC upon O incorporation were performed at 0 K. Hence, the suggested stability range of up to 18.75 at.% was based on enthalpy of formation alone [11]. However, at elevated temperatures effects from entropy and vibrations come into play, which may reduce the experimentally achievable amount of substitutional O. In fact, the configurational entropy reaches its maximum for the C:O ratio of 1:1, i.e., for 12.5 at.% O. This corresponds to the attained O content in Sample II, and is very close to the value obtained for Sample I. The two different synthesis routes used in the present paper, resulting in comparable amounts of incorporated O, further suggest that phase stability at elevated temperatures is mainly governed by the effects of entropy. 13 at.% of O may therefore be the maximum value attainable from the here used experimental conditions. Synthesis at lower temperatures may be attempted in order to suppress the entropy effects and thus stabilize $Ti_2Al(C_{1-x}O_x)$ with higher O concentrations, as long as the epitaxial growth conditions are retained.

The analysis of mechanical properties presented above, in combination with previously predicted anisotropic electronic properties strongly dependent on substitutional O [13], indicates an interesting material with tunable characteristics by means of varying the O concentration. $Ti_2Al(C_{1-x}O_x)$ is therefore highly promising for applications such as sliding electric contacts, where (tunable) conduction combined with low friction coefficient and good wear resistance is required.

5. Conclusions

Ab initio calculations on mechanical properties of $Ti_2Al(C_{1-x}O_x)$ predict a linear increase in ideal strength with increasing O content for [-1010](0001) and [1-210](0001) shear systems. Materials synthesis through O (from residual gas) incorporation during deposition of Ti_2AlC_y as well as solid-state reaction between understoichiometric TiC_y and Al_2O_3 substrates has also been performed. Compositional analysis of resulting single-crystal $Ti_2Al(C_{1-x}O_x)$ MAX phase reveals incorporation of up to 13 at.% O, consistent with theoretical predictions. The results demonstrate a highly promising material with predicted tunable electronic as well as mechanical properties.

Acknowledgements

The research leading to these results has received funding from the European Research Council under the European Community's Seventh Framework Programme (FP7/2007-2013)/ERC Grant agreements nº 258509 and 227754, and the Swedish Research Council (VR). The calculations were carried out using supercomputer resources provided by the Swedish National Infrastructure for Computing (SNIC) at the National Supercomputer center (NSC).

1. Nowotny H (1970) Struktuchemie einiger Verbindungen der Ubergangsmetalle mit den Elementen C, Si, Ge, Sn. Prog Solid State Chem 2:27-62
2. Barsoum MW, El-Raghy T (2001) The MAX Phases: Unique New Carbide and Nitride Materials. Am Sci 89 (4):334-343
3. Barsoum MW (2000) The M(N+1)AX(N) Phases: A New Class of Solids. Prog Solid State Chem 28:201-281
4. Radovic M, Barsoum MW, Ganguly A, Zhen T, Finkel P, Kalidindi SR, E. L-C (2006) On the elastic properties and mechanical damping of Ti3SiC2, Ti3GeC2, Ti3Si0.5Al0.5C2 and Ti2AlC in the 300-1573 K temperature range. Acta Mater 54:2757-2767
5. Meng FL, Zhou YC, Wang J (2005) Strengthening of Ti2AlC by substituting Ti with V. Scr Mater 53:1369-1372
6. Barsoum MW, Salama I, El-Raghy T, Golczewski J, Porter WD, Wang H, Seifert HJ, Aldinger F (2002) Thermal and Electrical Properties of Nb2AlC, (Ti,Nb)2AlC and Ti2AlC. Metall Mater Trans A 33A:2775-2779
7. Zhou Y, Meng F, Zhang J (2008) New MAX-Phase Compounds in the V-Cr-Al-C System Journal of the American Ceramic Society 91 (4):1357-1360
8. Barsoum MW, Ali M, El-Raghy T (2000) Processing and characterization of Ti2AlC, Ti2AlN, and Ti2AlC0.5N0.5. Metall Mater Trans A 31A (2):333-337
9. Rosen J, Persson POÅ, Ionescu M, Kondyurin A, McKenzie DR, Bilek MMM (2008) Oxygen incorporation in Ti_2AlC thin films. Appl Phys Lett 92:064102

10. Persson POÅ, Rosen J, McKenzie DR, Bilek MMM, Höglund C (2008) A solid phase reaction between TiC_x thin films and Al_2O_3 substrates. J Appl Phys 103:066102
11. Dahlqvist M, Alling B, Abrikosov IA, Rosen J (2010) Phase stability of Ti2AlC upon oxygen incorporation: A first principles investigation. Phys Rev B 81:024111
12. Liao T, Wang J, Li M, Zhou Y (2009) First-principles study of oxygen incorporation and migration mechanisms in Ti2AlC. J Mater Res 24 (10):3190-3196
13. Rosen J, Dahlqvist M, Simak SI, McKenzie DR, Bilek MMM (2010) Oxygen incorporation in Ti2AlC: Tuning of anisotropic conductivity. Appl Phys Lett 97:073103
14. Persson POÅ, Rosen J, McKenzie DR, M.M.M. B (2009) Formation of the MAX-phase oxycarbide Ti2AlC1-xOx studied via electron energy-loss spectroscopy and first-principles calculations. Phys Rev B 80:092102
15. Ryves L, Bilek MMM, Oates TWH, Tarrant RN, McKenzie DR, Burgmann FA, McCulloch DG (2005) Synthesis and in-situ ellipsometric monitoring of Ti/C nanostructured multilayers using a high-current, dual source pulsed cathodic arc. Thin Solid Films 482:133-137
16. Rosen J, Ryves L, Persson POÅ, Bilek MMM (2007) Deposition of epitaxial Ti_2AlC thin films by pulsed cathodic arc. J Appl Phys 101:056101
17. Bosman M, Keast VJ (2008) Optimizing EELS acquisition. Ultramicroscopy 108:837-846
18. Liao T, Wang J, Zhou Y (2008) Ab initio modelling of the formation and migration of monovacancies in Ti2AlC. Scr Mater 59:845-857
19. Kresse G, Hafner J (1994) Ab initio molecular-dynamics simulation of the liquid-metal amorphous-semiconductor transition in germanium. Phys Rev B 49 (20):14251-14269
20. Kresse G, Hafner J (1993) Ab initio molecular dynamics for open-shell transition metals. Phys Rev B 48 (17):13115-13118
21. Blöchl PE (1994) Projector augmented-wave method. Phys Rev B 50 (24):17953-17979
22. Perdew JP, Burke K, Ernzerhof M (1996) Generalized Gradient Approximation Made Simple. Phys Rev Lett 77 (18):3865-3868
23. Salama I, El-Raghy T, Barsoum MW (2002) Sythesis and mechanical properties of Nb2AlC and (Ti, Nb)2AlC. J Alloy Compd 347:271-278
24. Barsoum MW, Farber L, El-Raghy T (1999) Dislocations, Kink Bandsm and Room-Temperature Plasticity of Ti3SiC2. Metall Mater Trans A 30:1727-1738
25. Farber L, Barsoum MW, Zavaliangos A, El-Raghy T, Levin I (1998) Dislocations and Stacking Faults in Ti3SiC2. J Am Ceram Soc 81 (6):1677-1681
26. Liao T, Wang J, Zhou Y (2006) Deformation modes and ideal strengths of ternary layered Ti2AlC and Ti2AlN from first-principles calculations. Phys Rev B 73:214109
27. Liao T, Wang J, Zhou Y (2006) Basal-plane slip systems and polymorphic phase transformation in Ti2AlC and Ti2AlN: a first-principles study. J Phys: Condens Matter 18:6183-6192
28. T. Liao, Wang J, Zhou Y (2006) Basal-plane slip systems and polymorphic phase transformation in Ti2AlC and Ti2AlN: a first-principles study. J Phys: Condens Matter 18:6183-6192

Fig. 1 Low magnification and lattice resolved TEM images of the MAX phase structure in Sample I [(**a**) and (**c**)] and Sample II [(**b**) and (**d**)]

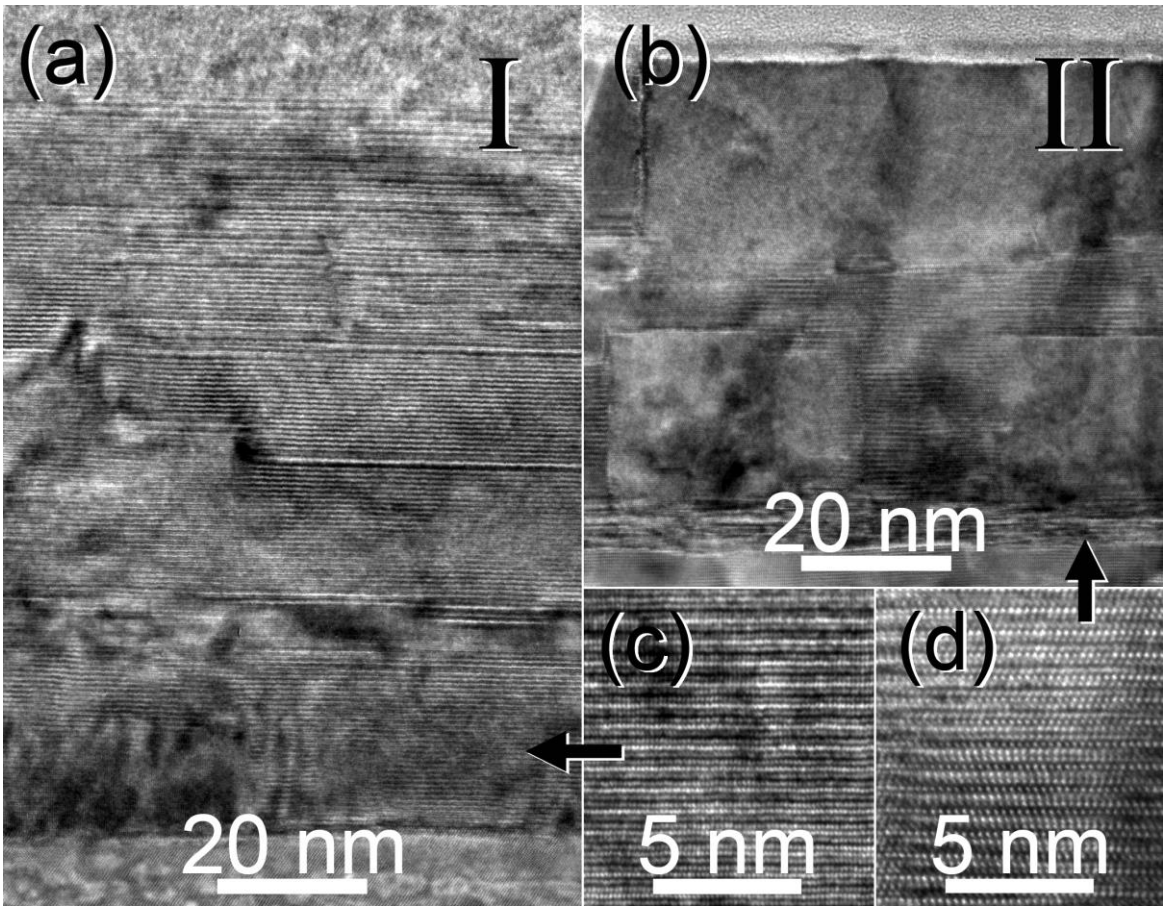

Fig. 2 Final EEL spectra from Sample I and II

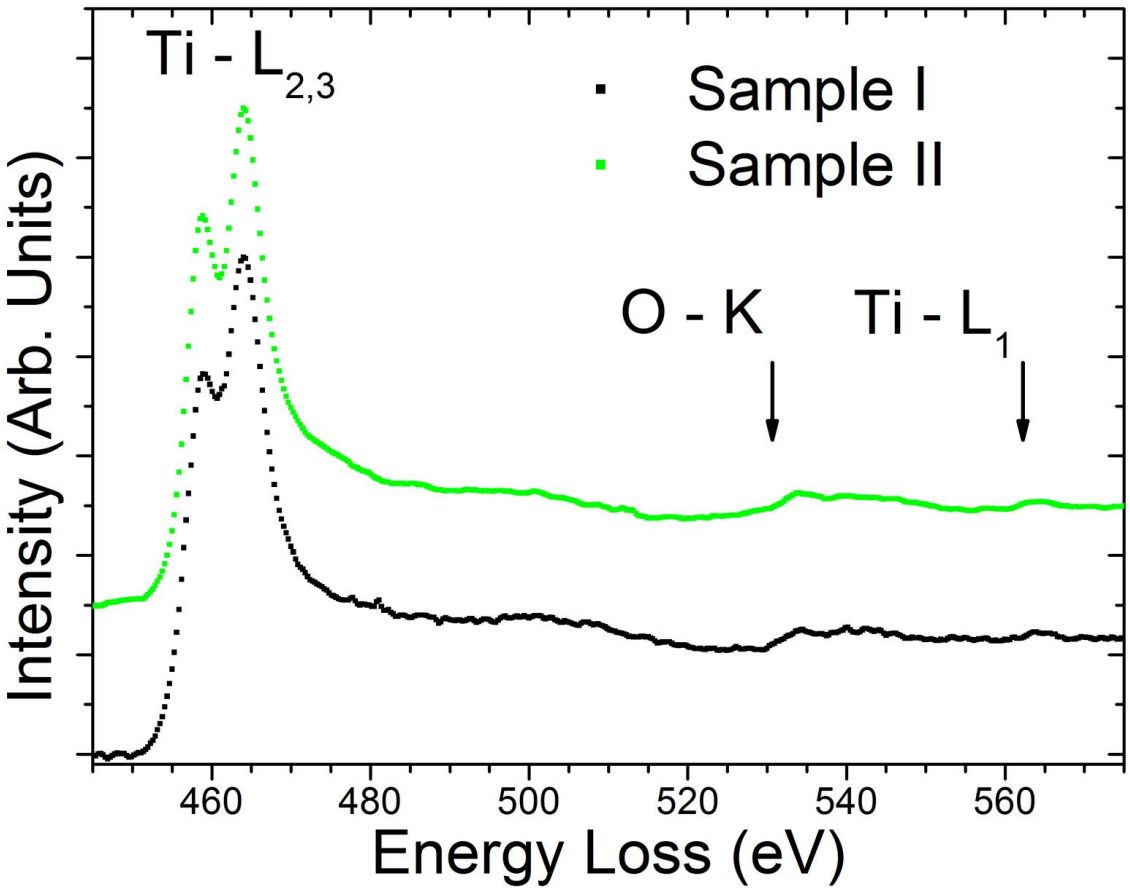

Fig. 3 (**a**) Calculated shear stresses as function of strain for [-1010](0001) and [1-210](0001) slip systems of $Ti_2Al(C_{1-x}O_x)$. Solid lines and filled symbols represent data for [-1010](0001) and dashed lines and open symbols data for [1-210](0001). X-symbols represent data from Liao *et al*.[28] (**b**) The Ti_6Al prism in top and side view. Evolution of Ti_6Al prism (top view) for (**c**) [-1010](0001) and (**d**) [1-210](0001) slip system upon applied strain along path I and II